MDPI

Article

Theoretical Evaluation of the Reinjection Probability Density Function in Chaotic Intermittency

Sergio Elaskar [1,*] and Ezequiel del Río [2]

1   Departamento de Aeronáutica, Instituto de Estudios Avanzados en Ingeniería y Tecnología (IDIT), FCEFyN, Universidad Nacional de Córdoba and CONICET, Córdoba 5000, Argentina
2   Departamento de Física Aplicada, ETSI de Aeronáutica y Espacio, Universidad Politécnica de Madrid, 28040 Madrid, Spain; ezequiel.delrio@upm.es
*   Correspondence: selaskar@unc.edu.ar

Abstract: The traditional theory of chaotic intermittency developed for return maps hypothesizes a uniform density of reinjected points from the chaotic zone to the laminar one. In the past few years, we have described how the reinjection probability density function (RPD) can be generalized as a power law function. Here, we introduce a broad and general analytical approach to determine the RPD function and other statistical variables, such as the characteristic relation traditionally utilized to characterize the chaotic intermittency type. The proposed theoretical methodology is simple to implement and includes previous studies as particular cases. It is compared with numerical data, the *M* function methodology, and the Perron–Frobenius technique, showing high accuracy between them.

Keywords: chaotic intermittency; maps; reinjection probability density function; continued fractions

1. Introduction

Chaos theory encompasses many fields of research [1]; one of them is the study of different routes to chaos [2,3]. Chaotic intermittency is a route by which a dynamic system can develop chaos. It is characterized by almost ordered motion in state space disrupted by randomly distributed chaotic bursts. Regular or laminar phases represent pseudo-equilibrium and pseudo-periodic solutions, while the bursts are related with chaotic behavior [2–9].

In the middle of the 20th century, Batchelor and Townsend utilized the intermittency word to represent the fluctuating velocity in fully turbulent flows [10]. Furthermore, in the 1970s, intermittency was also experimentally observed in developed turbulence [11]. In nonlinear dynamics and chaos, the intermittency concept was introduced by Pomeau and Maneville in the context of the Lorenz system [12]. Afterward, intermittency has been found in several phenomena in chemistry, engineering, physics, medicine, biology, etc. [13–29]. Accordingly, a deeper description of the chaotic intermittency phenomenon would increase the understanding of these topics.

Initially, chaotic intermittency was classified into three types: I, II, and III following the loss of stability of a periodic orbit or the loss of stability of a fixed point for the local Poincaré map [12,30]. After that, other types of chaotic intermittency were found: X, V, on–off, eyelet, ring, etc. [31–36].

Several continuous systems that contract volume in state spaces can be described by one-dimensional maps [37]. These maps are characterized by a local map and a reinjection process. The local map is defined around the unstable or vanished fixed point and determines the type of intermittency and the laminar dynamics. Type I intermittency happens by a tangent bifurcation when an eigenvalue of the map leaves the unit circle across +1. Type II intermittency occurs by a Hopf bifurcation, and two complex conjugate eigenvalues leave the unit circle. Type III intermittency appears by a subcritical period-doubling bifurcation,

and then an eigenvalue leaves the unit circle across -1 [2,3,6,7]. For intermittency types I, II, and III, the characteristic local maps are [6]

$$
\begin{aligned}
x_{n+1} &= \varepsilon + x_n + a\,x_n^p & \text{type I} \\
x_{n+1} &= (1+\varepsilon)\,x_n + a\,x_n^p & \text{type II} \\
x_{n+1} &= -(1+\varepsilon)\,x_n - a\,x_n^p & \text{type III}
\end{aligned}
\tag{1}
$$

where ε, a, and p are control parameters. $x_0 = 0$ is a fixed point for the three maps, and the laminar interval L is delimited around it.

The reinjection probability density function (RPD function) is utilized to describe the reinjection mechanism. This function determines the probability that trajectories are returned or reinjected close to the unstable or vanished fixed point and inside the laminar interval [2–4,6,7]. The RPD function is defined by the chaotic dynamics of the system and strongly influences the correct description of the chaotic intermittency. The RPD was determined using various methods, although a comprehensive methodology was not employed. Among the different approaches tested, the most commonly adopted hypothesis was uniform reinjection [2–4,30].

A novel theory has been formulated, enabling the assessment of the RPD function through either an analytical representation of a map or by utilizing a set of numerical or experimental data [38]. In this theory, the RPD function is described by a power law with exponent α, and it works correctly for types I, II, III, and V intermittency with and without noise [6,7]

$$
\phi(x) = b\,x^\alpha, \quad x \in L. \tag{2}
$$

The theory establishes that the reinjection process depends on the map derivative at pre-reinjection points, i.e., points x_n that verify $x_{n+i} = F^i(x_n)$ where $x_{n+i} \in L$, n, and i are integer numbers [6,39]. Therefore, the pre-reinjection points drive the reinjection process.

The new generalized RPD function includes the uniform reinjection as a particular case for $\alpha = 0$ [38]. Furthermore, as the characteristic relation depends on the RPD function, the new RPD introduces a generalization of the characteristic relation concept [6,7].

A non-uniform RPD function happens if the map derivative at pre-reinjection points is zero or tends to infinity [6,7]. In a previous paper, the RPD was analytically evaluated for a map derivative at pre-reinjection points equal to zero [39]. The authors approximate the map at pre-reinjection points as a power law function with exponent γ

$$
x_{n+1} = F(x_n) \cong F(x_r) + w\,(x_n - x_r)^\gamma, \tag{3}
$$

where w is an appropriate constant and the parameter γ determines the RPD function exponent

$$
\alpha = \frac{1}{\gamma} - 1. \tag{4}
$$

Therefore, to determine the RPD function, the key is the correct obtaining of the exponent γ. However, this scheme can exclusively be implemented at extreme pre-reinjection points, allowing γ only to acquire positive integer values. By the symmetry between a function and its inverse, this scheme was extended to include the following maps derivative

$$
\lim_{x \to x_r} \frac{d\,F(x)}{d\,x} \to \infty \tag{5}
$$

where x_r is a pre-reinjection point. However, the exponent γ results in $\gamma = 1/j$, where j is a positive integer [40].

This paper introduces a theory that generalizes the previous studies obtaining a comprehensive analytical approximation for the RPD function. In the new framework, the exponents γ and α are represented for simple continued fractions and can acquire any real number. Therefore, the previous developments are only particular cases of the

new theory. In addition, for several maps, the theory describes that continued fractions determine the characteristic relation exponent β.

Numerical tests are carried out to validate the new analytical results. Also, the new theory is compared with the M function methodology and the Perron–Frobenius operator technique [6,7,41]. In all the tests, the new theoretical results accurately verify the numerical ones. Additionally, they show good agreement with those calculated by the M function methodology and the Perron–Frobenius operator technique.

The present paper has five sections. After this introduction, in Section 2, we outline the previous works to evaluate the exponent γ. Section 3 describes the main result of this work, and we present a general analytical method to calculate the RPD function and the exponent of the characteristic relation β. Section 4 shows several numerical tests to compare the new analytical results with those numerically calculated. Finally, in the last section, we summarize the main conclusions.

2. The RPD Function

As explained in previous studies, the RPD function is determined by the nonlinear map that produces the reinjection mechanisms [6,39]. The theoretical description of the power law RPD function provided by Equation (2) works correctly for an extensive class of maps exhibiting chaotic intermittency with and without noise [6,7].

Here, we describe two previous studies to calculate the exponent γ [39,40]. In Section 3, we show that both works are only particular cases of the theory introduced in this paper.

We study one-dimensional maps

$$x_{n+1} = F(x_n), \ D \to D \tag{6}$$

where D is a real interval. $F(x)$ is a piecewise differentiable function and satisfies $|F'(x)| \neq 0$ and $|F'(x)| \nrightarrow \infty$ except at a finite number of points called critical points of the map.

To clarify concepts, let us consider a classical map [38,42]:

$$x_{n+1} = F(x_n) \equiv \begin{cases} F_1(x_n) = (1+\varepsilon)x_n + (1-\varepsilon)x_n^p, & x_n < x_r \\ \\ F_2(x_n) = (F_1(x_n) - 1)^\gamma, & x_n \geq x_r \end{cases} \tag{7}$$

where x_r verifies $F_1(x_r) = 1$, and γ is a real number. $F_1(x)$ determines the laminar behavior, and it is called the local map. On the other hand, $F_2(x)$ governs the reinjection process. $x_0 = 0$ is a fixed point for the map, which becomes unstable for $\varepsilon > 0$. Type II intermittency happens for $0 < \varepsilon \ll 1$.

In a fundamental paper, Manneville [42] determined uniform reinjection for Map (7) with $p = 2$ and $\gamma = 1$, whereas del Rio and Elaskar [38] presented the generalization to the map $F_2(x) = (F_1(x) - 1)^\gamma$ for different values of γ obtaining a power law RPD function.

All reinjected points inside the laminar zone $L = [x_0, c]$ come from points near to x_r. For $x_n \geq x_r$, all points in $(x_n, x_n + \Delta x_n)$ map on the interval $(F_2(x_n), F_2(x_n + \Delta x_n))$, where x_n are pre-reinjection points $x_n \in [x_r, F_2^{-1}(c)]$, and where $x_r = F_2^{-1}(x_0)$ and $c \ll 1$ is the upper limit of the laminar interval. Then, using the Perron–Frobenius operator methodology, the RPD function can be written as [6,41]

$$\phi(x) = \frac{k \rho(x_n)}{F_2'(x_n)} \tag{8}$$

where $x = F_2(x_n)$, $F_2'(x)$ is the derivative of the $F_2(x)$ function, and $\rho(x)$ is the trajectories density. A constant k is included because the density $\rho(x)$ is normalized in the interval $[0, 1]$ and the RPD function is only normalized in the laminar interval L: $\int_{x_0}^{c} \phi(\tau)d\tau = 1$.

If we introduce the map provided by Equation (7) in Equation (8), we obtain [38,39]

$$\phi(x) = \frac{k\,\rho(x_n)}{\gamma\,F_1'(x_n)}x^\alpha, \quad \alpha = \frac{1}{\gamma} - 1, \quad x \in [x_0, c] \tag{9}$$

where $F_1'(x) = dF_1(x)/dx$ can approximate as constant inside the interval $[x_r, F_2^{-1}(c)]$, and we assume the trajectories density $\rho(x)$ is also constant in the same interval. Therefore, the RPD results in a power law function with exponent $\alpha = \frac{1}{\gamma} - 1$. Note that Equation (9) reduces to Equation (2), where $b = \frac{k\,\rho(x_n)}{\gamma\,F_1'(x_n)}$.

The new framework RPD can be applied for maps with a more complicated reinjection process. To study it, we consider the following map [43]

$$x_{n+1} = F(x_n) = -(1+\varepsilon)\,x_n - a\,x_n^3 + d\,x_n^6\,\sin(x_n); \quad a > 0 \tag{10}$$

For $0 < \varepsilon \ll 1$, this map shows type III intermittency around the unstable fixed point $x_0 = 0$. The reinjection process depends on the value of $F(x_r)$ at the extreme points x_r verifying $dF(x)/dx|_{x_r} = 0$. As the number of iterations rises, points x_n near to $x_0 = 0$ move away in a process governed by the control parameters a and ε. For large values of x_n, the third term on the right-hand side of Equation (10) increases its impact and x_n approaches the maximum x_r, providing the reinjection in the laminar interval. Note that points in the neighborhood of x_r spend two iterations to be reinjected in the laminar zone; even so, for these types of maps, the RPD function is also provided by Equation (2). Accordingly, we can calculate from Equation (10) a value of the parameter γ determining the exponent α by Equation (9).

The power law RPD $\phi(x) = b\,x^\alpha$ was verified in an extended class of one-dimensional maps (see [6,7] and references listed there). In addition, the new theory incorporates the previous studies, which implement a constant RPD. The uniform RPD is only a particular case for $\gamma = 1$ and $\alpha = 0$. Otherwise, $\gamma \neq 1$ implies $\alpha \neq 0$.

A constant RPD is generated at pre-reinjection points with a non-zero and finite map derivative. On the other hand, if the RPD function is generated at pre-reinjection points where the map derivative is zero or tends to infinity, the parameter $\gamma \neq 1$ generates no uniform RPD, $\phi(x) = b\,x^\alpha$, with $\alpha = \frac{1}{\gamma} - 1 \neq 0$.

From Equation (9), five different behaviors are found depending on the α value:

- Case 1: $-1 < \alpha < 0$; $\infty > \gamma > 1$, and $\frac{d\phi(x)}{dx} < 0$ for $x \in L = [0, c]$.
- Case 2 (uniform reinjection): $\alpha = 0$, $\gamma = 1$, and $\frac{d\phi(x)}{dx} = 0$ for $x \in L = [0, c]$.
- Case 3: $0 < \alpha < 1$, $1 > \gamma > 1/2$, $\frac{d\phi(x)}{dx} > 0$, and $\frac{d^2\phi(x)}{dx^2} < 0$ for $x \in L = [0, c]$.
- Case 4: $\alpha = 1$, $\gamma = 1/2$, $\frac{d\phi(x)}{dx} > 0$, and $\frac{d^2\phi(x)}{dx^2} = 0$ for $x \in L = [0, c]$.
- Case 5: $1 < \alpha$, $\gamma < 1/2$, $\frac{d\phi(x)}{dx} > 0$, and $\frac{d^2\phi(x)}{dx^2} > 0$ for $x \in L = [0, c]$.

Note that, for Equation (2), the RPD functions x^α and $x^{1/\alpha}$ possess symmetry concerning the bisector line.

2.1. Map Derivative Is Equal to Zero at Pre-Reinjection Points

In this framework, where $\phi(x)$ is generated around the point x_r as Equation (9) describes, the parameter γ determines the exponent α of the RPD function. For most maps, the exponent γ does not appear explicitly in the map definition. Ref. [39] introduced a methodology to theoretically evaluate γ, which relates a value of γ to a reinjection map. Nevertheless, this methodology only applies to reinjection processes generated around extreme points. It implies that the γ exponent can only acquire positive integer values.

We briefly describe the theoretical methodology introduced in [39]. The map around an extreme point x_r is approximated by Equation (3): $F(x) \cong F(x_r) + w(x - x_r)^\gamma$. From this equation, γ can be obtained as

$$\gamma = q + \lim_{x \to x_r} F^{(q+1)}(x) \frac{x - x_r}{F^{(q)}(x)}. \tag{11}$$

where the exponent between parentheses shows the order of derivation. If the derivatives with $n \le q$ verify $F^{(n)} = 0$ and the derivative $F^{(q+1)} \ne 0$ and finite, the parameter γ results in $\gamma = q + 1$, and, from Equation (9), the exponent α is

$$\alpha = -\frac{q}{q+1}. \tag{12}$$

Accordingly, the RPD function results

$$\phi(x) = b \, x^{-\frac{q}{q+1}} = b \, x^\alpha, \tag{13}$$

where b is the normalization parameter

$$b = \frac{1}{\int_{x_0}^c x^\alpha \, dx}. \tag{14}$$

It is important to note that the formulation introduced in [39] cannot evaluate the RPD functions for $\alpha > 0$. Therefore, this scheme does not include Cases 3, 4, and 5.

2.2. Map Derivative Tends to Infinity at Pre-Reinjection Points

A method to calculate the exponents γ and α for maps with derivatives $lim_{x \to x_r} \frac{dF(x)}{dx} \to \infty$ has been presented in a recent paper [40]. This paper only studies maps like Equation (7) shows. Here, we extend this methodology to include more general maps like those provided by Equation (6).

Let us consider a map provided by Equation (6). It shows intermittency and $\lim_{x \to x_r} \frac{dF(x)}{dx} \to \infty$, where x_r is a pre-reinjection point. To determine the parameter γ and the exponent α, we use the inverse function of $y = F(x)$ around x_r. Geometrically, we are taking advantage of the symmetry concerning the bisector line of a function with its inverse.

Once the inverse function of $y = F(x)$ around x_r has been obtained, called here $V(y)$, we utilize the analytical method previously described to calculate the exponent γ_v for the inverse function. From Equation (3), the $V(y)$ function can be approximated as

$$V(y) \cong V(y_r) + w_q (y - y_r)^{\gamma_v}, \quad \gamma_v > 1 \tag{15}$$

where w_q is a constant, $y_r = F(x_r)$, and γ_v can be obtained using the Equation (11)

$$\gamma_v = q_v + \lim_{y \to y_r} V^{(q_v+1)}(y) \frac{y - y_r}{V^{(q)}(y)}. \tag{16}$$

If the derivatives of $V(y)$ at $y = y_r$ verify $V^{(i)}(y_r) = 0$ with $i \le q_v$ and $V^{(q_v+1)}(y_r) \ne 0$ and finite, then $\gamma_v = q_v + 1$. In view of that, the approximation of $F(x)$ can be calculated from Equations (3) and (15)

$$F(x) \propto (x - x_r)^{1/\gamma_v}. \tag{17}$$

Therefore, the RPD function is provided by Equation (13), with $\alpha = \frac{1}{\gamma} - 1 = \gamma_v - 1$.

We highlight that, to use this framework, $F(x)$ must be injective around x_r [44]. Also, this scheme applies to maps $y = F(x)$ for which there are no analytical inverse functions [40]. However, γ is restricted to rational numbers $1/j$, where j is an integer number.

To apply Equations (15) and (16), we have assumed that $V(y)$ is at least a C^{γ_v} scalar function around x_r [45]. Accordingly, we can use Taylor's Theorem [44]

$$V(y) \cong V(y_r) + (y - y_r) \left. \frac{dV(y)}{dy} \right|_{y_r} + \frac{(y-y_r)^2}{2!} \left. \frac{d^{(2)}V(y)}{dy^{(2)}} \right|_{y_r} + \ldots + \frac{(y-y_r)^{\gamma_v}}{\gamma_v!} \left. \frac{d^{(\gamma_v)}V(y)}{dy^{(\gamma_v)}} \right|_{y_r} + \ldots \quad (18)$$

As $V^{(1)}(y_r) = \ldots = V^{(\gamma_v-1)}(y_r) = 0$ and $V^{(\gamma_v)}(y_r) = V^{(q_v+1)}(y_r) \neq 0$, the last equation reduces to

$$V(y) \cong V(y_r) + \frac{(y - y_r)^{\gamma_v}}{\gamma_v!} \left. \frac{d^{(\gamma_v)}V(y)}{dy^{(\gamma_v)}} \right|_{y_r} + \ldots \quad (19)$$

The error is proportional to $|y - y_r|^{\gamma_v+1} = |y - y_r|^{q_v+2}$, where $|y - y_r| \ll 1$ because the laminar interval is also small: $|F^{-1}(x) - F^{-1}(x_r)| \ll 1$. Then, the lower-order non-zero derivative governs Series (18). Accordingly, this theory works accurately for $c \ll 1$.

3. Real Exponent

In the previous section, we studied the RPD evaluation for maps where the exponent γ is limited to integer numbers or rational numbers $1/j$, where j is an integer number.

Here, the formulation presented in Section 2 is extended to maps that can generate exponents γ and α represented by any real number (integer, rational, and irrational). At pre-reinjection points, the map derivatives verify

$$\left. \frac{d^{(j)}F(x)}{dx^{(j)}} \right|_{x_r} = 0, \quad j \leq q \quad \text{and} \quad \lim_{x \to x_r} \frac{d^{(q+1)}F(x)}{dx^{(q+1)}} \longrightarrow \infty \quad (20)$$

where q is an integer number, $q = 0, 1, 2 \ldots$. Therefore, from Equation (11), the limit

$$\gamma - q = \lim_{x \to x_r} F^{(q+1)}(x) \frac{x - x_r}{F^{(q)}(x)}. \quad (21)$$

is indeterminate. Note the theory developed in previous papers and described in Section 2 does not include these cases. To solve it, we approximate $F^{(q)}(x)$ as

$$F^{(q)}(x) \cong w (x - x_r)^{\gamma_{F(q)}}, \qquad \gamma_{F(q)} > 0. \quad (22)$$

Therefore, the derivative $F^{(q+1)}(x)$ results in

$$F^{(q+1)}(x) \cong w \, \gamma_{F(q)} (x - x_r)^{\gamma_{F(q)}-1}. \quad (23)$$

If we introduce Equations (22) and (23) into Equation (21), we obtain

$$\lim_{x \to x_r} F^{(q+1)}(x) \frac{x - x_r}{F^{(q)}(x)} \cong \gamma_{F(q)} \quad \Rightarrow \quad \gamma = q + \gamma_{F(q)}. \quad (24)$$

To evaluate $\gamma_{F(q)}$ (see Equation (22)) for maps $F(x)$ verifying $\lim\limits_{x \to x_r} F^{(q+1)}(x) \to \infty$ and $F^{(j)}(x) = 0$ for $j = 0, 1, 2 \ldots, q$, we calculate the inverse of $F^{(q)}(x)$ and approximate it by

$$V(y) = \left(F^{(q)} \right)^{-1}(y) \cong V(y_r) + w_q (y - y_r)^{\gamma_q}, \quad (25)$$

where $y_r = F^{(q)}(x_r)$, and γ_q is calculated by Equation (16). If the derivatives of $V(y)$ satisfy

$$V^{(j)}(y)\Big|_{y_r} = 0, \quad j = 1, 2 \dots, q_1$$

$$V^{(q_1+1)}(y)\Big|_{y_r} \neq 0, \text{ and finite}.$$

(26)

Therefore, using Equation (17), we obtain $\gamma_{F^{(q)}} = 1/\gamma_q$, where $\gamma_q = q_1 + 1$. Now, following Equations (21) and (24), the exponent γ results in

$$\lim_{x \to x_r} F^{(q+1)}(x) \frac{x - x_r}{F^{(q)}(x)} \cong \frac{1}{\gamma_q}, \quad \gamma = q + \frac{1}{\gamma_q}.$$

(27)

However, we could find that the derivatives $V^{(j)}(y_r)$ are zero for $j \leq q_1$ and the derivative $V^{(q_1+1)}(y)$ tends to infinity at y_r:

$$V^j(y)\Big|_{y_r} = 0, \quad j = 1, 2 \dots, q_1$$

$$\lim_{y \to y_r} V^{(q_1+1)}(y) \to \infty.$$

(28)

In this case, we cannot directly apply Equation (17). Then, we use Equation (22) and approximate the inverse function of $V^{(q_1)}(y)$ as

$$V_1(z) = \left(V^{(q_1)}\right)^{-1}(z) \cong V_1(z_r) + w_{q_1}(z - z_r)^{\gamma_{q_1}},$$

(29)

where $z_r = V^{(q_1)}(y_r)$ and w_{q_1} is a constant. If the derivatives of $V_1(z)$ verify

$$V_1^{(j)}(z)\Big|_{z_r} = 0, \quad j = 1, 2 \dots, q_2$$

$$V_1^{(q_2+1)}(z)\Big|_{z_r} \neq 0, \text{ and finite}.$$

(30)

Then, $\gamma_{v_1} = q_2 + 1$, and $V^{(q_1)}$ can be approximated by

$$V^{(q_1)}(y) \propto (y - y_r)^{\gamma_v} = (y - y_r)^{1/\gamma_{v_1}}.$$

(31)

Accordingly, the exponent γ results in (see Equation (27))

$$\gamma = q_0 + \frac{1}{q_1 + \frac{1}{\gamma_{q_1}}}.$$

(32)

Note that q in Equation (27) is called q_0 in Equation (32).

On the other hand, if $V_1(z)$ verifies Equation (28), we can generalize Equations (27) and (32) as follows

$$\gamma = q_0 + \frac{1}{q_1 + \frac{1}{q_2 + \frac{1}{q_3 + \frac{1}{\dots}}}}.$$

(33)

Consequently, a simple continued fraction determines the exponent γ, where q_i with $i = 1, 2, 3, \dots$ are positive integer numbers and q_0 is zero or a positive integer number.

Once γ is obtained, we can evaluate α using Equation (4). Therefore, the exponent α also can be written as a continued fraction

$$\alpha = -1 + \frac{1}{\gamma} = -1 + \frac{1}{q_0 + \frac{1}{q_1 + \frac{1}{q_2 + \frac{1}{q_3 + \frac{1}{\dots}}}}}.$$

(34)

Then, γ and α are determined by simple continued fractions [46,47].

$$\gamma = [q_0, q_1 \ldots, q_n], \qquad \alpha = [-1, q_0, q_1 \ldots, q_n], \tag{35}$$

where $q_0, q_1 \ldots$ are called partial quotients, and they depend on the map derivatives at pre-reinjection points.

If the simple continued fractions provided by Equation (35) are finite, α and γ are rational numbers. However, if Equation (35) includes infinite simple continued fractions, α and γ are irrational numbers [46,47]. Therefore, the γ and α exponents can acquire integer, rational, and irrational numbers. Accordingly, the dynamic of the non-linear reinjection map determines the exponents γ and α together with their associated continued fractions.

On the other hand, the characteristic relation determines the evolution of the average laminar length $\bar{l}$ as a function of the control parameter ε: $\bar{l} = \bar{l}(\varepsilon)$, where the average laminar length is

$$\bar{l} = \int_0^{l_m} \psi(l, c) l(x, c) dl = \int_{L(c)} \phi(x) l(x, c) dx \tag{36}$$

where $l(x, c)$ is the laminar length, l_m is the highest laminar length, and $L(c)$ is the laminar interval.

For type I, II, and III intermittencies, the characteristic relation can be written as $\bar{l} \propto \varepsilon^\beta$ [2,6,7]. For several cases, the exponent of the characteristic relation satisfies $\beta = \text{const} \, \alpha$ [6,7]. Accordingly, for these cases, β is also provided by a continued fraction.

We note that Equation (33) can be related to the Gauss map. We can write this equation as

$$\gamma = q_0 + \cfrac{1}{q_1 + \cfrac{1}{q_2 + \cfrac{1}{q_3 + \delta_{q_3}}}}, \tag{37}$$

where the sequence δ_{q_n} verifies

$$\delta_{q_{n+1}} = G(\delta_{q_n}) = \frac{1}{\delta_{q_n}} - \left[\frac{1}{\delta_{q_n}}\right] \tag{38}$$

where $\left[\frac{1}{\delta_n}\right]$ is the integer part of $\frac{1}{\delta_n}$. Equation (38) is the Gauss map [48,49].

If we relate Equations (37) and (38), we obtain the following relation

$$q_{n+1} = \frac{1}{\delta_{q_n}} - \delta_{q_{n+1}} = \frac{1}{\delta_{q_n}} - G(\delta_{q_n}) = \left[\frac{1}{\delta_{q_n}}\right]. \tag{39}$$

Therefore, once we know δ_{q_n}, we can calculate q_{n+1} and $\delta_{q_{n+1}}$, where the partial quotients q_n are the highest-order derivative equal to zero of the map.

Any irrational number has a unique representation by continued fractions. Accordingly, the golden mean $w^* = 0.5 \sqrt{5} - 1$ is described by a simple continued fraction. Let us define the following ratio

$$w_n = \frac{f_n}{f_{n+1}} = \cfrac{1}{1 + \cfrac{1}{1 + \cfrac{1}{1 + \ldots}}} \tag{40}$$

where f_n are the Fibonacci numbers [2]

$$f_{n+1} = f_n + f_{n-1}; \quad f_0 = 0, \, f_1 = 1 \quad n = 0, 1, 2 \ldots \tag{41}$$

From Equation (40), the golden mean can be calculated

$$w^* = \lim_{n \to \infty} w_n = \frac{1}{1 - w} = \frac{\sqrt{5} - 1}{2} \tag{42}$$

Let us analyze a particular case for the reinjection mechanism: $\gamma = \alpha$. Accordingly, the following equation must be satisfied

$$\alpha = \frac{1}{\alpha} - 1,\tag{43}$$

which possesses as a solution the golden mean w^*. Therefore, we obtain $\gamma = \alpha = w^*$.

On the other hand, the M function methodology establishes that the exponent α is [6,7,38]

$$\alpha = \frac{2\,m - 1}{1 - m},\tag{44}$$

where m is a free parameter that can be calculated from the data series. For the particular case $\alpha = m$, we find $\alpha = m = w^*$.

In consequence, for $\alpha = \gamma = m = w^*$, there is a particular reinjection process that generates the following RPD function

$$\phi(x) = b\,x^{w^*} \cong b\,x^{0.618033989}.\tag{45}$$

Indirect Reinjection Mechanism

We analyze the indirect reinjection process, in which pre-reinjection points spend more than one iteration to reinject in the laminar zone.

Let us start with points x_n close to a point with zero derivatives that need more than one interaction to reinject. Therefore, the map is a composition of functions

$$x_{n+1} = F(x_n) = F_s \circ F_{s-1} \circ F_{s-2} \ldots \circ F_1(x_n)\tag{46}$$

where $F_1(x)$ is the only function that possesses a point with zero derivative at x_r, which is mapped inside the laminar interval by consecutive application of the single functions F_i forming the complete map $F(x)$

$$\frac{d\,F_1(x_r)}{d\,x} = 0,\quad F(x_r) \in L\tag{47}$$

where L is the laminar interval.

In this case, the exponent γ to determine the complete RPD function is calculated by applying Equation (11) only to function $F_1(x)$ instead of using it regarding the composed map $F(x)$ [39].

Let us consider the indirect reinjection for the composed Map (46) when the function $F_1(x)$ verifies

$$\lim_{x \to x_r} \frac{d\,F_1(x)}{d\,x} \to \infty,\quad F(x_r) \in L.\tag{48}$$

Because the derivative tends to infinity at x_r, we have to use the inverse map of Equation (46), which is provided by

$$y_{n+1} = V(y_n) = V_1 \circ V_2 \ldots \circ V_{s-1} \circ V_s(y_n)\tag{49}$$

where the function $V_i(y)$ is the inverse of $F_i(x)$. The $V_1(y)$ function possesses an extreme point at $y_r = F(x_r)$, which corresponds with the infinite slope of the map at x_r. The other V_i functions with $i \neq 1$ do not have extreme points. To determine the exponents γ, α, and the RPD function for the composed Map (46), we analyze the function V_1 by applying the methodology described in this section.

4. Numerical Results

We introduce some numerical tests to verify the accuracy of the analytical method described in previous sections.

For a broad comparison, we study three maps with different laminar dynamics and reinjection mechanisms. The first one shows type I intermittency, but the second and third maps display type II intermittency. On the other hand, the first and second maps have one reinjection mechanism. However, the third map possesses two reinjection processes.

4.1. First Test

This test considers the following map

$$
F(x) \equiv
\begin{cases}
F_1(x) = \varepsilon + x + a\,x^p, & x < x_r \\[2em]
F_2(x) = \dfrac{\left(x\sqrt{1-\frac{\ln(x)}{\ln(x_r)}} - \dfrac{\sqrt{\pi}\,x_r\,\mathrm{erf}\left(\sqrt{1-\frac{\ln(x)}{\ln(x_r)}}\sqrt{\ln(x_r)}\right)}{2\sqrt{\ln(x_r)}}\right)}{1 - \sqrt{\pi}\,x_r\,\mathrm{erf}\left(\sqrt{\frac{\ln(x)}{\ln(x_r)}}\right)}, & x \ge x_r
\end{cases}
\tag{50}
$$

where x_r is calculated from $\varepsilon + x_r + a\,x_r^p = 1$, and $\mathrm{erf}(x)$ is the error function. For $\varepsilon = 0$, the map provided by Equation (50) has a fixed point at $x_0 = 0$. For $0 < \varepsilon \ll 1$, the fixed point vanishes, there is a channel between the map and the bisector, and type I intermittency occurs. Note that $F_1(x)$ is the local map, and $F_2(x)$ determines the reinjection mechanism. Figure 1 shows Map (50) for $a = 1$, $\varepsilon = 0.001$ and $p = 2$.
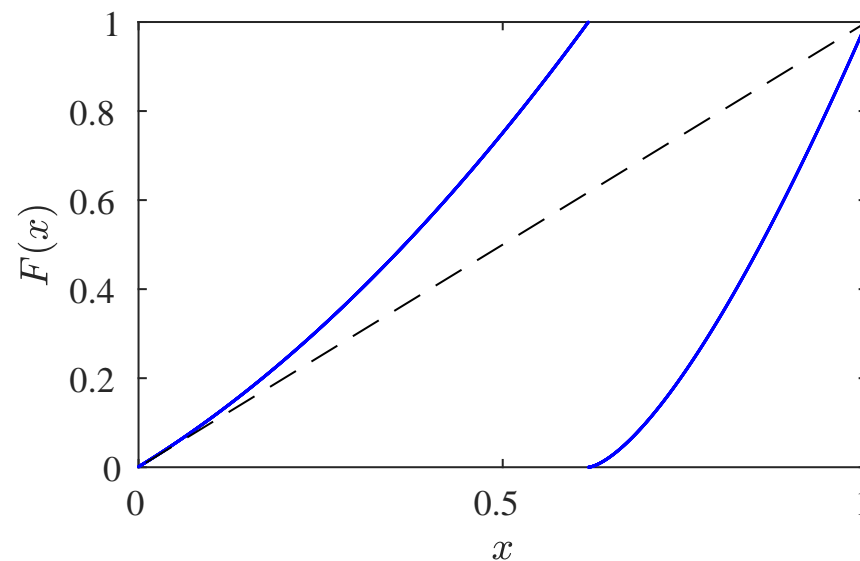

Figure 1. Map provided by Equation (50) for $a = 1$, $\varepsilon = 0.001$, and $p = 2$. Blue line: the map. Dashed black line: the bisector.

The first derivative of $F_2(x)$ in Equation (50) is

$$
\frac{d\,F_2(x)}{dx} = -\frac{2\sqrt{\ln(x_r) - \ln(x)}}{\sqrt{\pi}\,x_r\,\mathrm{erf}\left(\sqrt{\ln(x_r)}\right) - 2\sqrt{\ln(x_r)}}.
\tag{51}
$$

For $x = x_r$, it verifies $\left.\dfrac{d\,F_2(x)}{dx}\right|_{x_r} = 0$.

We highlight that Equation (51) is similar to Equation (21) of Ref. [40]. However, there is a fundamental conceptual difference. Equation (21) of Ref. [40] is directly the map. On the other hand, Equation (51) is the map derivative. Therefore, we use Equation (50) to show that the methodology described in Ref. [40] is only a particular case of the theory introduced in this work.

The second derivative of $F_2(x)$ results in

$$\frac{d^2 F_2(x)}{dx^2} = -\frac{x^{-1}\left(\sqrt{\ln(x_r) - \ln(x)}\right)^{-1}}{\sqrt{\pi}\,x_r\,\text{erf}\left(\sqrt{\ln(x_r)}\right) - 2\sqrt{\ln(x_r)}}, \tag{52}$$

which verifies $\lim_{x \to x_r} \frac{d^2 F_2(x)}{dx^2} \to \infty$. Therefore, we cannot directly apply the theory developed in previous papers. We have to use the analytical method described in Section 3. From Equations (33), (51), and (52), we deduce that $q_0 = 1$ and $1 < \gamma < 2$.

We calculate the inverse function of $\frac{d F_2(x)}{dx}$

$$V(y) = \left(\frac{d F_2(x)}{dx}\right)^{-1} = x_r^{1-(y/k)^2} \tag{53}$$

where k is

$$k = \frac{2\sqrt{\ln(x_r)}}{x_r\sqrt{\pi}\,\text{erf}\left(\sqrt{\ln(x_r)}\right) - 2\sqrt{\ln(x_r)}}. \tag{54}$$

Note that $y_r = \frac{d F_2(x)}{dx}\Big|_{x_r} = 0$.

The first derivative of $V(y)$ is

$$\frac{d V(y)}{d y} = -\frac{2 x_r^{1-(y/k)^2}\, y\, \ln(x_r)}{k^2}. \tag{55}$$

Then, $\frac{d V(y)}{d y}\Big|_{y_r} = 0$. Then, we have to calculate the second derivative of $V(y)$

$$\frac{d^2 V(y)}{d y^2} = -\frac{2 x_r^{1-(y/k)^2}\, \ln(x_r)\left(k^2 - 2 y^2\, \ln(x_r)\right)}{k^4}. \tag{56}$$

Therefore, $\frac{d^2 V(y)}{d y^2}\Big|_{y_r} \neq 0$ and finite. Accordingly, it implies $\gamma_v = 2$ and $\gamma_{F_2^{(1)}} = 1/\gamma_v = 1/2$. From Equation (33), we obtain

$$\gamma = q_0 + \frac{1}{q_1} = 1 + \frac{1}{\gamma_v} = 1 + \frac{1}{2} = \frac{3}{2} \tag{57}$$

and, using Equation (9), the exponent α is evaluated

$$\alpha = -1 + \frac{1}{\gamma} = -1 + \frac{1}{q_0 + \frac{1}{q_1}} = -\frac{1}{3}. \tag{58}$$

Then, by applying Equation (35), we can write

$$\gamma = [1, 2], \qquad \alpha = [-1, 1, 2]. \tag{59}$$

Finally, for a laminar interval $L = [0, c]$, the RPD function results in

$$\phi(x) = \frac{\alpha + 1}{c^{\alpha+1}}\, x^\alpha. \tag{60}$$

To verify these results, we carry out numerical tests. We use $a = 1$, $c = 0.025$, and $N = 80{,}000$, where N is the number of reinjected points (which is obtained after millions of iterations). To obtain the numerical data, first, we produce an iterative process using Map

(50). Later, we split the laminar interval L into N_s sub-intervals, and, finally, we calculate the reinjection histogram and the numerical RPD function. In this test, we use $N_s = 500$.

Also, to compare with the new theoretical results, we implement the M function methodology. We calculate the parameter m and the exponent α_M [6]. The RPD evaluated by the M function methodology results in

$$\phi_M(x) = \frac{\alpha_M + 1}{c^{\alpha_M + 1}} x^{\alpha_M}. \tag{61}$$

To calculate Equation (61), we have utilized the function $M(x)$, which is defined as

$$M(x) = \begin{cases} \dfrac{\int_{x_s}^{x} \tau\, \phi(\tau)\, d\tau}{\int_{x_s}^{x} \phi(\tau)\, d\tau} & \text{if } \int_{x_s}^{x} \phi(\tau) d\tau \neq 0, \\[4mm] 0 & \text{if } \int_{x_s}^{x} \phi(\tau) d\tau = 0, \end{cases} \tag{62}$$

where $x_s < x$ for all reinjected points x. Note that the function $M(x)$ can be calculated as the average of reinjection points in the interval $[x_s, x]$. Then, if we sort the reinjection points following the relation $x_j < x_{j+1}$, a very simple evaluation of the function $M(x)$ can be obtained

$$M(x_l) = \frac{\sum_{j=1}^{l} x_j}{l}. \tag{63}$$

We emphasize that, to apply Equation (63), we do not need to know the function $\phi(x)$. For the RPD provided by Equation (61), $M(x)$ is a linear function [6,38]

$$M(x) = m\,x, \quad x > x_s \tag{64}$$

where α_M in Equation (61) depends on the slope m

$$\alpha_M = \frac{2\,m - 1}{1 - m}. \tag{65}$$

The M function methodology finds $\alpha_M = -0.343$, which is very close to the analytical result provided by Equation (58). The relative percentage difference is $e_\alpha = 100 \frac{\alpha_M - \alpha}{\alpha_M} < 3\%$.

Figure 2 shows the RPD functions obtained using the M function methodology, the analytical method described in this paper, and the numerical results. We can observe that the three RPDs are very close. Also, $\phi(x)$ and $\phi_M(x)$, provided by Equations (60) and (61), respectively, verify with high accuracy the numerical data.

To analyze the difference between numerical data and the RPD functions obtained by the new method and those provided by the M function methodology, we calculate

$$D_r = \sqrt{\frac{\sum_{j=1}^{j=N_s} \frac{(\phi_t(j) - \phi_n(j))^2}{(\phi_t(j))^2}}{N_s^2}}, \qquad E_r = \frac{\sum_{j=1}^{j=N_s} \frac{|\phi_t(j) - \phi_n(j)|}{\phi_t(j)}}{N_s}, \tag{66}$$

where $\phi_n(j)$ is the numerical RPD in the sub-interval j, and $\phi_t(j)$ is the RPD calculated by the new framework or by the M function methodology. The results are in Table 1. We can observe good agreement between the analytical RPDs with the numerical data. We note that, for small c, the new analytical method approaches slightly better the numerical data than the M function methodology.

After obtaining the RPD function, we can calculate the characteristic relation for Map (50), $\bar{l} \propto \varepsilon^\beta$. From Ref. [6] with $p = 2$ and $-1 < \alpha < 0$, we obtain $\beta = \alpha/2$. Accordingly, β is also provided by a generalized continued fraction

$$\beta_t = [-1/2, 1/2, 1] = -\frac{1}{6}. \tag{67}$$

We evaluate numerically the average laminar length, $\bar{l}$, for $\varepsilon = 1 \times 10^{-7} - 1 \times 10^{-13}$. The numerical exponent results in $\beta_n \cong -0.18$, which is close to the exponent analytically obtained (see Equation (67)). We highlight that the numerical results verify $\beta_n \to \beta_t$ for $\varepsilon \to 0$.

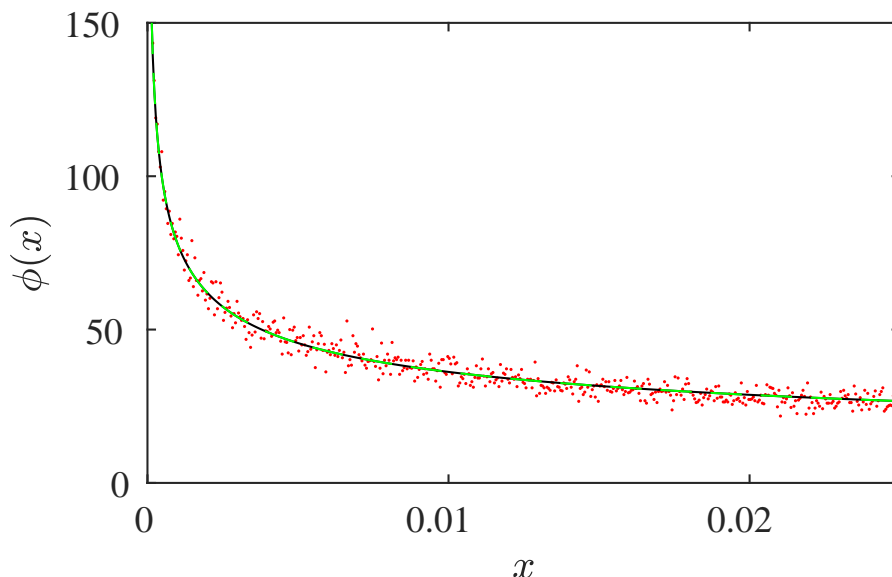**Figure 2.** Map (50). Comparison between the RPD functions for $a = 1$, $\varepsilon = 0.001$, $p = 2$, and $c = 0.025$. Red points: numerical RPD. Dashed green line: RPD calculated by the M function methodology. Blue line: theoretical RPD evaluated by Equation (60).

Table 1. D_r and E_r for the map provided by Equation (50). $N = 100,000$, $\varepsilon = 0.001$, $a = 1$, $p = 2$, $c = 0.025$.

	D_r	E_r
M function	3.944968×10^{-3}	$7.01789627 \times 10^{-2}$
Theory	3.439094×10^{-3}	$6.06325347 \times 10^{-2}$

4.2. Second Test

The second test analyzes the following map

$$F(x) \equiv \begin{cases} F_1(x) = (1+\varepsilon)\,x + a\,x^p, & x < x_r \\[2mm] \begin{aligned} F_2(x) = & \left(3(e^{x-x_r}-1) - \ln\left(1+(e^{x-x_r})^{1/3}\right)\right. \\ & -\sqrt{3}\,\arctan\left(\frac{-1+2(1-e^{x-x_r})^{1/3}}{\sqrt{3}}\right) \\ & \left. +\tfrac{1}{2}\ln\left(1-(e^{x-x_r})^{1/3}+(e^{x-x_r}-1)^{2/3}\right) - \frac{\pi}{2\sqrt{3}}\right)h, \end{aligned} & x \geq x_r \end{cases} \tag{68}$$

where x_r is calculated from $(1+\varepsilon)\,x_r + a\,x_r^p = 1$ and h is a constant provided by

$$h^{-1} = \left(3(e^{1-x_r}-1) - \ln\left(1+(e^{1-x_r})^{1/3}\right) - \sqrt{3}\,\arctan\left(\frac{-1+2(1-e^{1-x_r})^{1/3}}{\sqrt{3}}\right)\right. \\ \left. +\tfrac{1}{2}\ln\left(1-(e^{1-x_r})^{1/3}+(e^{1-x_r}-1)^{2/3}\right) - \frac{\pi}{2\sqrt{3}}\right). \tag{69}$$

For $\varepsilon = 0$, Equation (68) has a fixed point at $x_0 = 0$. For $0 < \varepsilon \ll 1$, the fixed point becomes unstable and type II intermittency occurs. Again, $F_1(x)$ is the local map,

and $F_2(x)$ governs the reinjection mechanism. Figure 3 shows the map for $a = 1$, $\varepsilon = 0.0001$, and $p = 2$.
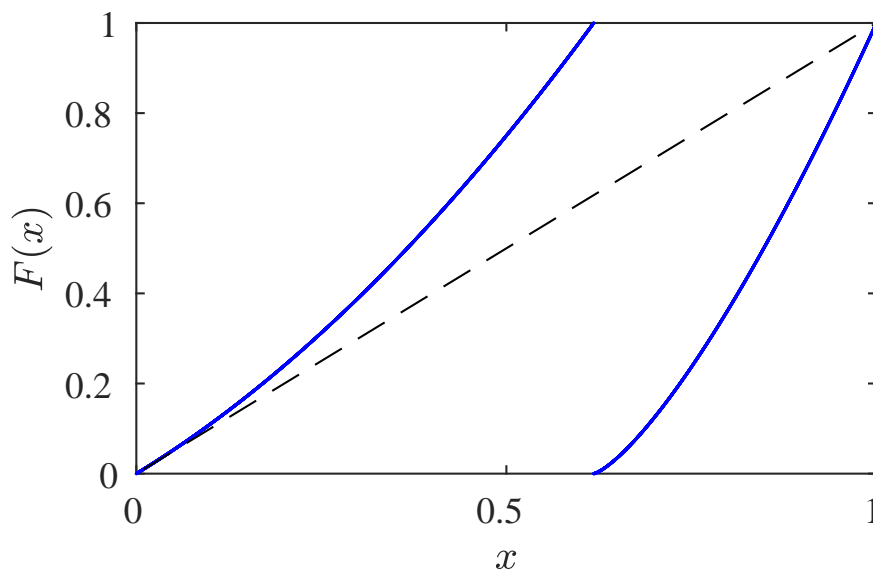

Figure 3. Map provided by Equation (68), $a = 1$, $\varepsilon = 0.0001$, and $p = 2$. Blue line: the map. Dashed black line: the bisector.

The first derivative of $F_2(x)$ is

$$\frac{d\,F_2(x)}{d\,x} = h\left(e^{x-x_r} - 1\right)^{1/3}. \tag{70}$$

Note that $\left.\frac{d\,F_2(x)}{d\,x}\right|_{x_r} = 0$. The second derivative of $F_2(x)$ is

$$\frac{d^2\,F_2(x)}{d\,x^2} = \frac{h\,e^{x-x_r}}{3\left(e^{x-x_r} - 1\right)^{2/3}}. \tag{71}$$

It verifies $\lim\limits_{x \to x_r} \frac{d^2\,F_2(x)}{d\,x^2} \to \infty$. Therefore, we can deduce that $q_0 = 1$ and $1 < \gamma < 2$.

To evaluate γ, we calculate the inverse function of $y = \frac{d\,F(x)}{d\,x}$, which results in

$$V(y) = \left(\frac{d\,F(x)}{d\,x}\right)^{-1} = x_r + \ln\left(1 + \frac{y^3}{h^3}\right). \tag{72}$$

The derivatives of this function, for $y_r = 0$, are

$$\left.\frac{dV(y)}{dy}\right|_{y_r} = 0, \quad \left.\frac{d^2V(y)}{dy^2}\right|_{y_r} = 0, \quad \left.\frac{d^3V(y)}{dy^3}\right|_{y_r} \neq 0 \text{ and finite}. \tag{73}$$

Then, $\gamma_v = 3$ and $\gamma_{F_2^{(1)}} = 1/3$. Now, we can calculate γ and α

$$\gamma = q_0 + \frac{1}{q_1} = 1 + \frac{1}{\gamma_v} = 1 + \frac{1}{3} = \frac{4}{3}. \tag{74}$$

By Equation (34), the exponent α results in

$$\alpha = -1 + \frac{1}{\gamma} = -1 + \frac{1}{q_0 + \frac{1}{q_1}} = -\frac{1}{4}. \tag{75}$$

Then, we can write

$$\gamma = [1,3], \qquad \alpha = [-1,1,3].\tag{76}$$

To validate these results, we develop computational tests. We calculate α numerically and by the M function methodology. Figure 4 shows the RPD functions for $a = 1$, $\varepsilon = 0.0001$, $p = 2$, and $c = 0.02$. Points are the numerical data, the black line is the RPD calculated analytically ($\alpha = -1/4$), and the dashed green line is the RPD obtained by the M function methodology.

The M function methodology obtains $\alpha_M = -0.2548$; therefore, the percentage difference results in $e_\alpha = 1.88\%$.
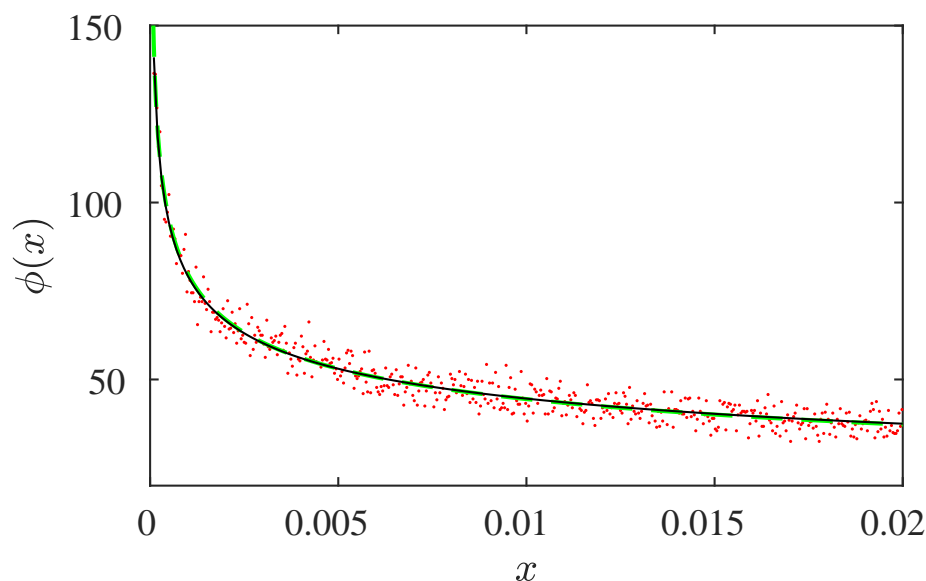

Figure 4. Equation (68). Comparison between the RPD functions for $a = 1$, $\varepsilon = 0.0001$, $p = 2$, and $c = 0.02$. Red points: numerical RPD. Dashed green line: RPD calculated by the M function methodology. Black line: theoretical RPD with $\alpha = -1/4$.

We calculate D_r and E_r for the RPD functions using Equation (66). The results are in Table 2. We can observe that both RPD functions have accuracy with the numerical data. Again, the new analytical RPD approaches slightly better the numerical results than the RPD calculated by the M function methodology.

Table 2. D_r and E_r for the map provided by Equation (50). $N = 100,000$, $\varepsilon = 0.0001$, $a = 1$, $p = 2$, $c = 0.02$.

	D_r	E_r
M function	3.0698612×10^{-3}	5.5695538×10^{-2}
Theory	3.0650469×10^{-3}	5.5637473×10^{-2}

As the theory considers the limit $x \to x_r$, the accuracy between α_M and α should increase when c decreases. We carry out several numerical tests and calculate the percentage difference, e_α. The results are shown in Table 3. Note that the agreement between α and α_M increases as c decreases.

Table 3. $N = 100{,}000$, $\varepsilon = 0.0001$, $a = 1$, $p = 2$.

c	α	α_M	e_α
0.02	−0.25	−0.2548	1.88%
0.05	−0.25	−0.2633	5.05%
0.10	−0.25	−0.2800	10.71%
0.20	−0.25	−0.2964	15.65%

The characteristic relation for Map (68) with $p = 2$ and $-1 < \alpha < 0$ has the following form: $\bar{l} \propto \varepsilon^\alpha$ (type II intermittency) [6]. Accordingly, β is provided by

$$\beta_t = \alpha = [-1, 1, 3] = -\frac{1}{4}. \tag{77}$$

We calculate the numerical average laminar length $\bar{l}$ for ε from 1×10^{-4} to 1×10^{-9}, and the exponent results in $\beta_n \cong -0.249$, very close to the theoretical $\beta_t = -0.25$ provided by Equation (77).

4.3. Third Test

For the last test, we consider a map with two reinjection processes

$$F(x) \equiv \begin{cases} F_1(x) = (1 + \varepsilon)x + a\,x^p, & 0 \le x < x_r \\[2mm] F_2(x) = (F_1(x) - 1)^\delta, & x_r \le x < x_z \\[2mm] F_3(x) = \left(1 + \ln\left(\frac{1}{x^{1/\ln(x_r)}}\right)\right)^\theta, & x_z \le x \le 1 \end{cases} \tag{78}$$

where x_r verifies $(1 + \varepsilon)x_r + a\,x_r^p = 1$, and $x_r < x_z \le 1$. For $\varepsilon = 0$, the map provided by Equation (78) has a fixed point $x_0 = 0$. For $0 < \varepsilon \ll 1$, the fixed point becomes unstable, and type II intermittency happens. The local map is determined by $F_1(x)$. However, $F_2(x)$ and $F_3(x)$ govern the reinjection mechanism. Figure 5 shows the map for $a = 3$, $\varepsilon = 0.001$, $p = 2$, $\delta = 0.4$, and $\theta = 2/3$.
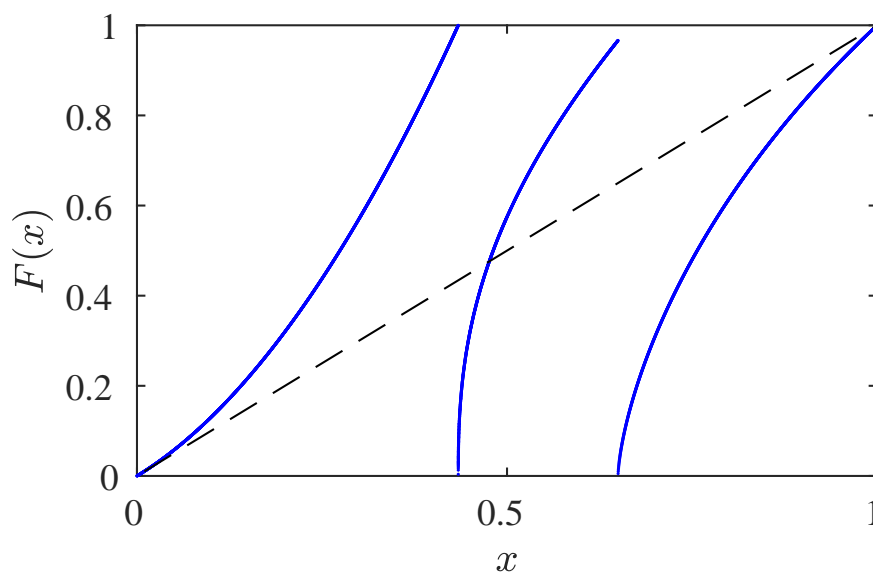

Figure 5. Map provided by Equation (78) for $\varepsilon = 0.001$, $a = 3$, $\delta = 0.4$, $\theta = 2/3$, $c = 0.1$, $p = 2$, and $x_z = 0.65$. Blue line: the map. Dashed black line: the bisector.

Note $F_2(x)$ and $F_3(x)$ generate two different reinjection processes. The map determined by $F_1(x)$ and $F_2(x)$ is a generalization of the traditional map introduced by Manneville [42], which was studied using the M function methodology in [38].

We analyze the two reinjection mechanisms separately and calculate the RPD function by adding these processes [6]. We start with the reinjection generated for $F_2(x)$ with $\delta = 0.4$. We apply the analytical framework developed in Section 3. We find

$$\lim_{x \to x_r} \frac{dF_2(x)}{dx} \to \infty \tag{79}$$

which implies $q_0 = 0$, and $0 < \gamma < 1$. The inverse function of $F_2(x)$ is

$$V(y) = \frac{-1 - \varepsilon + \sqrt{(1+\varepsilon)^2 + 4\,a\,(1 + y^{5/2})}}{2\,a}. \tag{80}$$

From this equation, we obtain

$$\left. \frac{d\,V(y)}{d\,y} \right|_{y_r} = 0; \quad \left. \frac{d^2\,V(y)}{d\,y^3} \right|_{y_r} = 0; \quad \lim_{y \to y_r} \frac{d^3\,V(y)}{d\,y^3} \to \infty \tag{81}$$

where $y_r = F_2(x_r)$. From Equation (81), we obtain $q_1 = 2$. Now, we have to calculate the inverse function $V_1(z) = \left(\frac{d^2\,V(y)}{d\,y^2} \right)^{-1}$ and its derivatives

$$\left. \frac{d\,V_1(z)}{dz} \right|_{z_r} = \left. \frac{1}{\frac{d^3 V(y)}{dy^3}} \right|_{y_r} = 0 \tag{82}$$

$$\left. \frac{d^2 V_1(z)}{dz^2} \right|_{z_r} = - \left. \frac{\frac{d^4 V(y)}{dy^4}}{\left(\frac{d^3 V(y)}{dy^3} \right)^3} \right|_{y_r} = 0 \tag{83}$$

$$\left. \frac{d^3 V_1(z)}{dz^3} \right|_{z_r} = \left. 3 \frac{\left(\frac{d^4 V(y)}{dy^4} \right)^2}{\left(\frac{d^3 V(y)}{dy^3} \right)^5} - \frac{\frac{d^5 V(y)}{dy^5}}{\left(\frac{d^3 V(y)}{dy^3} \right)^4} \right|_{y_r} \neq 0 \text{ and finite}, \tag{84}$$

where $z_r = \left. \frac{d^2\,V(y)}{d\,y^2} \right|_{y_r}$. From Equations (82)–(84), we found $q_2 = 2$.

The exponents γ_{F_2} and α_{F_2} are calculated by Equations (33) and (34)

$$\gamma_{F_2} = [0, 2, 2] = \frac{1}{2 + \frac{1}{2}} = \frac{2}{5}, \tag{85}$$

and

$$\alpha_{F_2} = [-1, 0, 2, 2] = -1 + \frac{1}{\frac{1}{2 + \frac{1}{2}}} = \frac{3}{2}. \tag{86}$$

To evaluate the second reinjection process, we analyze $F_3(x)$. The first derivative of $F_3(x)$ is

$$\frac{d\,F_3(x)}{d\,x} = - \frac{\theta \left(1 + \ln \left(\frac{1}{x^{1/\ln(x_r)}} \right) \right)^{\theta - 1}}{x \, \ln(x_r)}. \tag{87}$$

For $\theta < 1$, we obtain

$$\lim_{x \to x_r} \frac{d\,F_3(x)}{d\,x} \to \infty. \tag{88}$$

From this equation, we find $q_0 = 0$. Then, we have to calculate the inverse function of $F_3(x)$

$$V(y) = x_r^{1-y^{1/\theta}}. \tag{89}$$

Note that $y_r = F_3(x_r) = 0$. The derivative of $V(y)$ is

$$\frac{dV(y)}{dy} = -\frac{x_r^{1-y^{1/\theta}} \, y^{\frac{1}{\theta}-1} \, \ln(x_r)}{\theta}. \tag{90}$$

From this last equation, we obtain

$$\left.\frac{dV(y)}{dy}\right|_{y_r=0} = 0, \qquad \lim_{y \to y_r} \frac{d^2 V(y)}{dy^2} \to \infty. \tag{91}$$

From the Equation (91), we find $q_1 = 1$.

We call $V_1(z) = \left(\frac{dV(y)}{dy}\right)^{-1}$ and we use $\varepsilon = 0.001$, $a = 1$, $p = 2$, and $\theta = 2/3$. To determine the derivatives of $V_1(z)$, we use

$$\left.\frac{d\,V_1(z)}{dz}\right|_{z_r} = \left.\frac{1}{\frac{d^2 V(y)}{dy^2}}\right|_{y_r} = 0 \tag{92}$$

$$\left.\frac{d^2 V_1(z)}{dz^2}\right|_{z_r} = -\left.\frac{\frac{d^3 V(y)}{dy^3}}{\left(\frac{d^2 V(y)}{dy^2}\right)^3}\right|_{y_r} \neq 0 \text{ and finite}. \tag{93}$$

Therefore, we obtain $q_2 = 2$. The exponents γ_{F_3} and α_{F_3} are calculated by Equations (33) and (34)

$$\gamma_{F_3} = [0, 1, 2] = \frac{1}{1 + \frac{1}{2}} = \frac{2}{3}, \tag{94}$$

$$\alpha_{F_3} = [-1, 0, 1, 2] = -1 + \frac{1}{\frac{1}{1+\frac{1}{2}}} = \frac{1}{2}. \tag{95}$$

The complete reinjection process (the RPD function) is obtained by the addition of each contribution of $F_2(x)$ and $F_3(x)$ functions

$$\phi(x) = b\left(x^{\alpha_{F_2}} + x^{\alpha_{F_3}}\right) \tag{96}$$

where b is calculated from the normalization condition

$$b = \frac{(\alpha_{F_2}+1)(\alpha_{F_3}+1)}{c^{\alpha_{F_2}+1}(\alpha_{F_3}+1) + c^{\alpha_{F_3}+1}(\alpha_{F_2}+1)} \tag{97}$$

To verify the accuracy of Equations (96) and (97), we perform several tests to compare these equations with numerical data and the RPDs obtained by using the M function methodology and the Perron–Frobenius operator technique [41,50]. We utilize the following parameters: $\varepsilon = 0.001$, $a = 3$, $\delta = 0.4$, $\theta = 2/3$, $c = 0.1$, $p = 2$, $x_z = 0.65$, and $N = 250{,}000$. For these values, we obtain $x_r = 0.6179284$. Figure 6 displays the RPD functions. Red points are the numerical data. The dashed blue line is the RPD calculated using the M function methodology with two contributions (two α). The dashed magenta line is the RPD obtained by the M function methodology using only one contribution (one α). The green points are the RPD calculated by the Perron–Frobenius operator technique, and the black line is the RPD evaluation from Equations (96) and (97). The figure shows high accuracy between the RPD functions and numerical data.
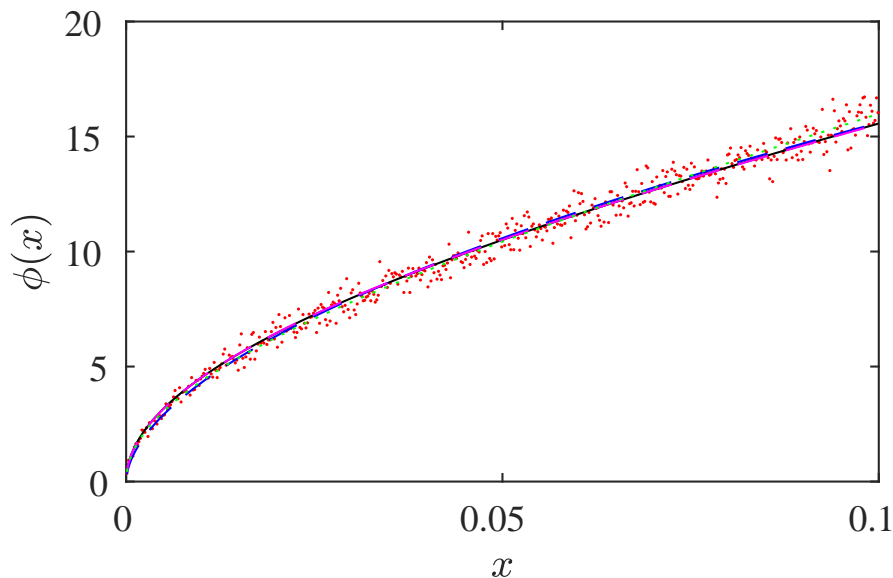
Figure 6. Comparison between the RPD functions for $\varepsilon = 0.001$, $a = 3$, $\delta = 0.4$, $\theta = 2/3$, $c = 0.1$, $p = 2$, $x_z = 0.65$, and $N = 250,000$. Red points: numerical RPD. Dashed blue line: RPD calculated by the M function methodology using two contributions. Dashed magenta line: RPD calculated by the M function methodology using one contribution. Green points: theoretical RPD calculated using the Perron–Frobenius operator. Black line: theoretical evaluation using Equations (96) and (97).

The differences between numerical data and the RPD functions calculated by the new method, the M function methodology (using one and two contributions), and the Perron–Frobenius operator technique are in Table 4. We note that all RPD functions show accuracy with the numerical data. However, the M function methodology with only one α shows the worst result.

Table 4. D_r and E_r for the map provided by Equation (78). $N = 250,000$, $\varepsilon = 0.001$, $a = 3$, $p = 2$, $c = 0.1$.

	D_r	E_r
M one contribution	2.629546×10^{-3}	4.138744×10^{-2}
M two contributions	2.233368×10^{-3}	3.854898×10^{-2}
Perron–Frobenius	2.234401×10^{-3}	3.782073×10^{-2}
Theory	2.235191×10^{-3}	3.845706×10^{-2}

The characteristic relation for type II intermittency depends on the α values. For this test, the exponents α generated by $F_2(x)$ and $F_3(x)$ are positive: $\alpha_{F_2} > 0$ and $\alpha_{F_3} > 0$. Therefore, they verify the relation $\alpha > p - 2$, where $p = 2$. In this case, following Ref. [6], we obtain $\beta_{F_2} = \beta_{F_3} = 0$, and the characteristic relation can be written as $\bar{l} = $ const.

To verify this result, we evaluate numerically the average laminar for ε from 1×10^{-4} to 1×10^{-9}. We find $\bar{l}_m \cong $ const in agreement with the theoretical evaluation.

5. Conclusions

Based on the well-confirmed results for several one-dimensional maps, the reinjection probability density function can be approached by the power law provided by Equation (2). In this work, we analyze how that RPD function is generated in return maps. We show that the non-uniform RPD is generated around pre-reinjection points where the map derivative verifies $\left.\frac{dF(x)}{dx}\right|_{x_r} = 0$ or $\lim_{x \to x_r} \frac{dF(x)}{dx} \to \infty$. Based on this fact, we present an analytical

methodology providing the RPD function; henceforth, by simple calculus, it is possible to evaluate the RPD function provided by Equation (2). In particular, we propose a scheme that provides the exponent α without any restriction on the possible values of it.

Once the exponent α is obtained, the value of the characteristic relation exponent β is also calculated. This analytical estimation is compared with numerical results showing good agreement between both.

The exponent α depends on the return map at pre-reinjection points. From Equation (9), α is a function of the parameter γ. Therefore, to describe the reinjection mechanism is necessary to calculate the exponent γ. We introduce a methodology to evaluate γ directly from the map, which includes the previous studies as particular cases. The new scheme allows γ and α to acquire any real number.

Additionally, this paper relates the continued fractions with the reinjection process in chaotic intermittency. The exponents γ and α are provided by simple continued fractions. Furthermore, the exponent of the characteristic relation β can be defined by continued fractions.

We find two general cases:

1. Let $F(x)$ be a one-dimensional map defined by Equation (6). If, for a positive integer q, $F^{(i)}(x_r) = 0$ with $i \leq q$ and $F^{(q+1)}(x_r) \neq 0$ and finite, the exponent $\gamma = q + 1$ is an integer number.
2. Let $F(x)$ be a one-dimensional map defined by Equation (6). If, for a positive integer q, $F^{(i)}(x_r) = 0$ with $i \leq q$ and $\lim\limits_{x \to x_r} \frac{d^{(q+1)}F(x)}{dx^{(q+1)}} \to \infty$, the exponent γ is a non-integer real number with $[\gamma] = q$.

Also, we can establish:

3. Let $F(x)$ be a one-dimensional map defined by Equation (6). If $\lim\limits_{x \to x_r} \frac{dF(x)}{dx} \to \infty$, the exponent γ is a real number that verifies $0 < \gamma < 1$.
4. Let $V(y)$ be a function defined by Equation (25). If, for a positive integer q, $V^{(i)}(y_r) = 0$ with $i \leq q$ and $\lim\limits_{y \to y_r} \frac{d^{(q+1)}V(y)}{dy^{(q+1)}} \to \infty$, a new partial quotient is added in Equation (34).
5. Let $F(x)$ be a one-dimensional map defined by Equation (6). A constant RPD function is recovered if the map derivative at pre-reinjection points is different to zero and finite.

Three numerical studies for different maps validate the new methodology. Two maps show type II intermittency and the third has type I intermittency. On the other hand, two maps have only one reinjection mechanism, and the remaining map possesses two reinjection processes. Aside from this, we compare the new theoretical results with those calculated by validated methodologies such as the M function and the Perron–Frobenius operator technique. The new theory works very accurately in all tests.

We highlight that only with the map equation the new theory allows us to evaluate the fundamental statistical variables for describing chaotic intermittency. If we know the map, we do not need to work with numerical or experimental data series to understand the intermittency behavior.

Note that the laminar map determines the intermittencies type. On the other hand, the chaotic zone of the map specifies the RPD function. Therefore, the new methodology could be utilized in systems possessing other intermittencies.

Author Contributions: Conceptualization, S.E.; methodology, S.E. and E.d.R.; formal analysis, S.E.; investigation, S.E. and E.d.R.; resources, S.E. and E.d.R.; writing—original draft preparation, S.E. and E.d.R.; writing—review and editing, S.E. and E.d.R.; supervision, S.E.; project administration, S.E. and E.d.R.; funding acquisition, S.E. and E.d.R. All authors have read and agreed to the published version of the manuscript.

Abbreviations

The following abbreviations are used in this manuscript:

RPD   Reinjection probability density function (form the chaotic region into the laminar one)

References

1. Elaskar, S. Symmetry in Nonlinear Dynamics and Chaos. *Symmetry* **2023**, *15*, 102. [CrossRef]
2. Schuster, H.; Just, W. *Deterministic Chaos*; Wiley VCH: Mörlenbach, Germany, 2005.
3. Nayfeh, A.; Balachandran, B. *Applied Nonlinear Dynamics*; Wiley: New York, NY, USA, 1995.
4. Marek, M.; Schreiber, I. *Chaotic Behaviour of Deterministic Dissipative Systems*; Cambridge University Press: Cambridge, UK, 1995.
5. Strogatz, S. *Nonlinear Dynamics and Chaos*; Perseus Book Publishing: Cambridge, UK, 1994.
6. Elaskar, S.; del Rio, E. *New Advances on Chaotic Intermittency and Applications*; Springer: New York, NY, USA, 2017; ISBN 978–3-319-47836-4.
7. Elaskar, S.; del Rio, E. Review of Chaotic Intermittency. *Symmetry* **2023**, *15*, 1195. [CrossRef]
8. Rasband, S. *Chaotic Dynamics of Nonlinear Dynamics*; John Wiley & Sons: New York, NY, USA, 1990.
9. Guckenheimer, J.; Holmes, P. *Nonlinear Oscillations, Dynamical Systems, and Bifurcations of Vector Field*; Springer: New York, NY, USA, 1983.
10. Batchelor, G.; Townsend, C. The nature of turbulent motion at large wave-number. *Proc. R. Soc. Lond. Ser. A* **1949**, *199*, 238–255.
11. Kuo, A.; Corrsin, S. Experiments on internal intermittency and fine-structure distribution functions in fully turbulent fluid. *J. Fluid Mech.* **1971**, *50*, 285–319. [CrossRef]
12. Manneville, P.; Pomeau, Y. Intermittency and Lorenz model. *Phys. Lett. A* **1979**, *75*, 1–2. [CrossRef]
13. Irimiciuc, S.; Saviuc, A.; Tudose-Sandu-Ville, F.; Toma, S.; Nedeff, F.; Marcela Rusu, C.; Agop, M. Non-Linear Behaviors of Transient Periodic Plasma Dynamics in a Multifractal Paradigm. *Symmetry* **2020**, *12*, 1356. [CrossRef]
14. Stavrinides, S.; Miliou, A.; Laopoulos, T.; Anagnostopoulos, A. The intermittency route to chaos of an electronic digital oscillator. *Int. J. Bifurc. Chaos* **2008**, *18*, 1561–1566. [CrossRef]
15. Schmiegel, J.; Pons, F. Stochastic Intermittency Fields in a von Kármán Experiment. *Symmetry* **2021**, *13*, 1752. [CrossRef]
16. Pizza, G.; Frouzakis, C.; Mantzaras, J. Chaotic dynamics in premixed Hydrogen/air channel flow combustion. *Combust. Theor. Model* **2012**, *16*, 275–299. [CrossRef]
17. Chian, A. *Complex System Approach to Economic Dynamics. Lecture Notes in Economics and Mathematical Systems*; Springer: Berlin/Heidelberg, Germany, 2007.
18. Bhansali, R.; Holland, M.; Kokoszka, P. Intermittency, long-memory and financial returns. In *Long Memory in Economics*; Springer: Berlin/Heidelberg, Germany, 2007; pp. 39–68.
19. Zebrowski, J.; Baranowski, R. Type-I intermittency in nonstationary systems: Models and human heart-rate variability. *Physical A* **2004**, *336*, 74–86. [CrossRef]
20. Paradisi, P.; Allegrini, P.; Gemignani, A.; Laurino, M.; Menicucci, D.; Piarulli, A. Scaling and intermittency of brains events as a manifestation of consciousness. *AIP Conf. Proc.* **2012**, *1510*, 151–161.
21. Bashkirtseva, I.; Nasyrova, V.; Ryashko, L. Scaling and intermittency of brains events as a manifestation of consciousness. *Chaos Solitons Fractals* **2018**, *110*, 76–81.
22. Suzuki, Y.; Lu, M.; Ben-Jacob, E.; Onuchic, J. Periodic, quasi-periodic and chaotic dynamics in simple gene elements with time delays. *Sci. Rep.* **2016**, *6*, 21037. [CrossRef] [PubMed]
23. Gardiner, J.; Atema, J. The function of bilateral odor arrival time differences in olfactory orientation of sharks. *Curr. Biol.* **2010**, *20*, 1187–1191. [CrossRef] [PubMed]
24. Atema, J.; Brönmark, C.; Hansson, L. Aquatic odor dispersal fields: Opportunities and limits of detection, communication and navigation. In *Chemical Ecology in Aquatic Systems*; Oxford University Press: New York, NY, USA, 2012; pp. 1–18.
25. Pawar, S.; Vishnu, R.; Vadivukkarasan, M.; Panchagnula, M.; Sujith, R. Intermittency route to combustion instability in a laboratory spray combustor. *J. Eng. Gas Turbine Power* **2016**, *138*, 041505-1. [CrossRef]

26. Nishiura, Y.; Ueyama, D.; Yanagita, T. Chaotic pulses for discrete reaction diffusion systems. *SIAM J. App. Dyn. Syst.* **2005**, *4*, 723–754. [CrossRef]

27. de Anna, P.; Le Borgne, T.; Dentz, M.; Tartakovsky, A.; Bolster, D.; Davy, P. Flow intermittency, dispersion and correlated continuous time random walks in porous media. *Phys. Rev. Lett.* **2013**, *110*, 184502.

28. Stan, C.; Cristescu, C.; Dimitriu, D. Analysis of the intermittency behavior in a low-temperature discharge plasma by recurrence plot quantification. *Phys. Plasmas* **2010**, *17*, 042115. [CrossRef]

29. Malasoma, J.; Werny, P.; Boiron, M. Multichannel type-I intermittency in two models of Rayleigh-Benard convection. *Phys. Rev. Lett.* **2004**, *51*, 487–500.

30. Hirsch, J.; Huberman, B.; Scalapino, D. Theory of intermittency. *Phys. Rev. Lett.* **1982**, *25*, 519–532.

31. Price, T.; Mullin, P. An experimental observation of a new type of intermittency. *Physical D* **1991**, *48*, 29–52. [CrossRef]

32. Platt, N.; Spiegel, E.; Tresser, C. On-off intermittency: A mechanism for bursting. *Phys. Rev. Lett.* **1993**, *70*, 279–282. [CrossRef]

33. Pikovsky, A.; Osipov, G.; Rosenblum, M.; Zaks, M.; Kurths, J. Attractor–repeller collision and eyelet intermittency at the transition to phase synchronization. *Phys. Rev. Lett.* **1997**, *79*, 47–50. [CrossRef]

34. Lee, K.; Kwak, Y.; Lim, T. Phase jumps near a phase synchronization transition in systems of two coupled chaotic oscillators. *Phys. Rev. Lett.* **1998**, *81*, 321–324. [CrossRef]

35. Bauer, M.; Habip, S.; He, D.; Martiessen, W. New type of intermittency in discontinuous maps. *Phys. Rev. Lett.* **1992**, *68*, 1625–1628. [CrossRef] [PubMed]

36. He, D.; Bauer, M.; Habip, S.; Kruger, U.; Martiessen, W.; Christiansen, B.; Wang, B. Type V intermittency. *Phys. Lett. A* **1992**, *171*, 61–65. [CrossRef]

37. Ott, E. *Chaos in Dynamical Systems*; Cambridge University Press: Cambridge, UK, 2008.

38. del Rio, E.; Elaskar, S. New characteristic relation in type-II intermittency. *Int. J. Bifurc. Chaos* **2010**, *20*, 1185–1191. [CrossRef]

39. del Rio, E.; Elaskar, S. On the theory of intermittency in 1D maps. *Int. J. Bifurc. Chaos* **2016**, *26*, 1650228. [CrossRef]

40. Elaskar, S.; del Rio, E.; Lorenzon, D. Chaotic intermittency in maps with infinite derivative. In Proceedings of the 2020 IEEE Congreso Bienal de Argentina (ARGENCON), Resistencia, Argentina, 1–4 December 2020; Published as IEEE Xplore 9505502.

41. Elaskar, S.; del Rio, E.; Zapico, E. Evaluation of the statistical properties for type-II intermittency using the Perron-Frobenius operator. *Nonlinear Dyn.* **2016**, *86*, 1107–1116. [CrossRef]

42. Manneville, P. Intermittency, self-similarity and $1/f$ spectrum in dissipative dynamical systems. *J. Phys.* **1980**, *41*, 1235–1243. [CrossRef]

43. Elaskar, S.; del Rio, E.; Donoso, J. Reinjection probability density in type-III intermittency. *Physical A* **2011**, *390*, 2759–2768. [CrossRef]

44. Bartle, R. *The Elements of Real Analysis*; John Wiley & Sons: New York, NY, USA, 1976.

45. Elaskar, S.; del Rio, E.; Gutierrez Marcantoni, L. Analytical evaluation of the reinjection probability density function in chaotic intermittency. In Proceedings of the 2020 IEEE Biennial Congress of Argentina, ARGENCON 2020, Resistencia, Argentina, 1–4 December 2020; Published as IEEE Xplore 9505540.

46. Murillo Tsijli, M. Sobre las fracciones continuas: Aplicaciones y curiosidades. *Matemática Educ. Internet* **2015**, *15*. [CrossRef]

47. Hensley, D. *Continued Fractions*; Word Scientific: Hackensack, NJ, USA, 2006.

48. Corless, R. Continued Fractions and Chaos. *Am. Math. Mon.* **1992**, *99*, 203–215. [CrossRef]

49. Pronzato, L.; Wynn, H.; Z Higljavsky, A. Analysis of performance of symmetric second-order line search algorithms through continued fractions. *IMA J. Math. Control Inf.* **2001**, *18*, 281–296. [CrossRef]

50. Elaskar, S.; del Rio, E.; Schulz, W. Analysis of the Type V Intermittency Using the Perron-Frobenius Operator. *Symmetry* **2022**, *14*, 2519. [CrossRef]